Twenty-Seventh Symposium (International) on Combustion/The Combustion Institute, 1998/pp. 2275–2282

# HOMOGENEOUS IGNITION OF METHANE-AIR MIXTURES OVER PLATINUM: COMPARISON OF MEASUREMENTS AND DETAILED NUMERICAL PREDICTIONS

URS DOGWILER, JOHN MANTZARAS, PETER BENZ, BEAT KAEPPELI, ROLF BOMBACH AND ANDREAS ARNOLD

*Paul Scherrer Institute*
*Combustion Research*
*CH-5232 Villigen-PSI, Switzerland*

The homogeneous ignition of lean methane-air mixtures was investigated numerically and experimentally in a laminar plane channel flow configuration established by two externally heated catalytically active (Pt-coated) ceramic plates, 250 mm long by 100 mm wide, placed 7 mm apart. Preheated fuel-air mixtures with equivalence ratios of 0.31 and 0.37 and uniform velocities of 1 and 2 m/s were examined, resulting in incoming Reynolds numbers ranging from 190 to 380. Planar laser-induced fluorescence (PLIF) was used to map the OH concentration field along the streamwise direction and thermocouples to monitor both catalyst plate temperatures. The numerical predictions included a two-dimensional elliptic model with detailed heterogeneous and homogeneous chemical reactions. The homogeneous ignition location strongly depends on the incoming velocity and mildly on the equivalence ratio. Following homogeneous ignition, a very stable V-shaped flame is formed in all cases. Measured and predicted flame sweep angles, OH levels, and the post-flame OH relaxation are in good agreement with each other, while the homogeneous ignition distance is predicted within 9% in all cases. The homogeneous ignition location is shown to be better identified with changes of averaged (over the channel cross section) quantities rather than with changes in local wall gradients. The overall model performance suggests that the employed surface scheme is capable of capturing the coupling between surface and gaseous chemistries leading to homogeneous ignition. Experiments and predictions were also carried out with noncatalytic plates. The resulting flame is unstable and asymmetric, clearly showing the stability advantages of catalytically assisted combustion.

## Introduction

Catalytically stabilized thermal combustion (CST) offers stable combustion of very lean fuel-air mixtures with high-power density and very low pollutant formation. In the last years, major efforts were directed in the numerical investigation of CST in one-dimensional stagnation point flow [1,2] and two-dimensional flat plate [3,4] or channel flow [5,6] configurations. Channel flows are the most relevant for practical CST applications (catalytic combustors are of the honeycomb type consisting of a multitude of catalytic channels). As detailed surface mechanisms for fuel oxidation over Pt or Pd catalysts have become available in the last years [7,8], their application in conjunction with full gaseous chemistry is crucial in understanding the heterogeneous–homogeneous interactions in practical combustors. In particular, issues such as the effect of radical adsorption or desorption on gas-phase ignition and stabilization can be only accounted with detailed gaseous and surface chemistries.

Recently [9], we investigated numerically CST of a lean (equivalence ratio $\varphi = 0.40$) methane-air mixture in a plane channel laminar flow using a model that included, for the first time, all relevant parameters: two-dimensional elliptic modeling with detailed gaseous and surface chemistries, radiative heat transfer from the hot catalyst surfaces, and one-dimensional heat conduction inside the solid plates. The key heterogeneous reactions influencing homogeneous ignition were identified; OH adsorption and desorption was found to play an important role on homogeneous ignition by strongly influencing its location. In the present work, we undertake a combined numerical and experimental CST study of lean methane-air mixtures in plane channel flows with the main objective to validate the numerical model. Additional objectives were to examine the influence of inlet velocity and mixture equivalence ratio on homogeneous ignition by performing parametric studies. Planar laser-induced fluorescence (PLIF) is used to map the OH concentration along the streamwise direction and thermocouples to monitor the catalyst surface temperature in a plane channel with Pt-coated walls.

The experimental arrangement is initially given, a

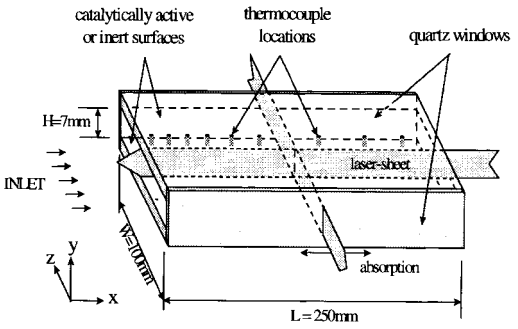


FIG. 1. Schematic of the catalytic burner geometry and the laser sheet configuration.

brief description of the numerical model follows, and then experimental and numerical results are presented for three cases with catalytically active surfaces and finally for one case with inert surfaces.

## Experimental

### *Burner Geometry*

Figure 1 shows a schematic of the catalytic channel combustor. It consists of two horizontal Si[SiC] ceramic plates 250 mm long, 100 mm wide, and 8 mm thick that are placed 7 mm apart. The other two channel surfaces are formed by two 3-mm-thick quartz windows that are spring pressed against the ceramic plates with a 0.5-mm-thick soft ceramic gasket placed in between to assure a leak-proof construction. The inner horizontal ceramic plate surfaces were made catalytically active by sputtering a 1-$\mu$m-thick nonporous $Al_2O_3$ layer on the Si[SiC] support followed by a 2-$\mu$m-thick Pt layer. The catalyst surface temperature along the streamwise axis of symmetry was measured by S-type thermocouples (14 for each plate) embedded 1 mm beneath the catalytically active surfaces through 1-mm-diameter by 7-mm-deep holes drilled from the outer horizontal plate surfaces. Given the high thermal conductivity of Si[SiC] (35 W/mK at 1300 K), these temperatures reflect within a few degrees the actual catalyst temperature. The catalyst plate temperatures were controlled independently by two 10-kW resistance-type heaters whose coils were wound 3 cm above the outer plate horizontal surfaces and were held in place by a ceramic enclosure. The incoming air flow was preheated and then mixed with $CH_4$ in a static mixer placed 300 mm upstream of the channel entrance. The preheated $CH_4$-air mixture passed first through a 20-mm-long section filled with metallic spheres 2 mm in diameter and then through a 50-mm-long inert honeycomb section (2 $\times$ 2 mm individual channel cross section) placed just upstream of the channel entrance to assure a nearly uniform incoming velocity profile. An additional retractable thermocouple was placed just downstream the honeycomb section to monitor the inlet temperature; it was withdrawn during actual operation to avoid any flow disturbances. The air and methane flows were regulated with two BROOKS mass flow meters.

### *Laser Diagnostics*

A frequency-doubled Nd:YAG laser (Quantel YG781C20) operated at 20 Hz pumped a tunable dye laser (Quantel TDL50 with dye a mixture of rhodamine 6G and rhodamine B). Its frequency-doubled radiation (285 nm) was transformed into a laser sheet by a cylindrical lens telescope and a 1-mm slit mask. The laser sheet was vertical (see Fig. 1) with a height of 5 cm and entered the channel along the plane of symmetry from the outlet. Because only the central part (7 mm) of the entire sheet height was used, the laser sheet had a nearly uniform intensity distribution within the measuring area; a very small divergence of the laser sheet was introduced along its propagation direction to assure accessibility up to the wall surfaces. The light sheet pulse energy was 0.5 mJ, low enough to avoid saturation of the P1(7) $A(v' = 1) \leftarrow X(v'' = 0)$ transition of the OH radical. The $(1 \rightarrow 1)$ and $(0 \rightarrow 0)$ fluorescence at 308 and 314 nm was recorded at 90° through one of the quartz windows with an intensified camera (Princeton Instruments ICCD-576S) equipped with a 105-mm focal length *f*/4.5 lens (Nikon UV Nikkor). Laser stray light was blocked off by a WG-295 absorption glass filter. The CCD camera was gated to as short a time as possible (165 ns) in order to minimize interference from the intense thermal radiation of the catalyst plates. The OH PLIF was calibrated with absorption measurements carried out with the laser sheet in the transverse direction where through optical access via the quartz windows is possible; transverse PLIF images were recorded by the same CCD via a mirror positioned at the channel outlet at 45° with respect to the streamwise axis.

## Numerical Model

The basic features of the numerical model (developed in Ref. [9]) are given next. It is a full elliptic two-dimensional model for a steady, laminar, two-dimensional gaseous reactive flow with the additional presence of surface reactions. The CHEMKIN database is used to evaluate gaseous transport properties. The species molecular transport considers the mixture average diffusivity as well as thermal diffusion for the light species [10]. For gaseous chemistry, the C/H/O mechanism by Warnatz and Maas [11] is used; only C1 chemistry is considered, a reasonable simplification for the very lean conditions of this study. In total, 100 reactions (46 reversible and 8 irreversible) and 16 species (excluding the

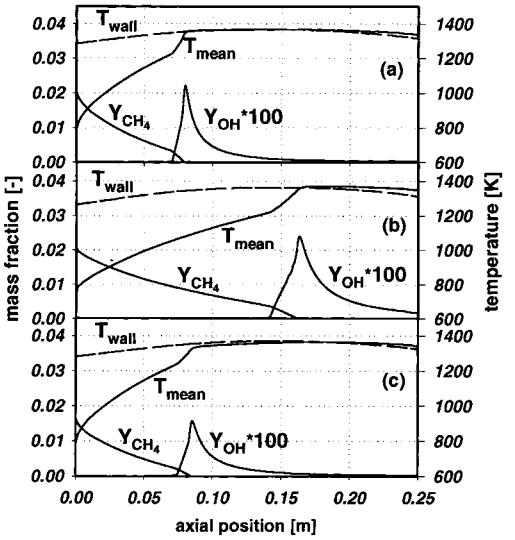


FIG. 2. Streamwise profiles of measured wall temperature and computed mean temperature, mean methane mass fraction, and mean OH mass fraction for cases (a), (b), and (c).

carrier nitrogen) are included. For surface chemistry, the reaction mechanism by Deutschmann et al. [12] was employed that included 26 reactions (20 irreversible and 3 reversible), 7 gaseous species, and 10 surface species (excluding Pt). The thermochemical data needed to calculate the equilibrium constants for the 3 reversible reactions of the surface mechanism were taken from Warnatz et al. [13]. The catalyst site density was taken as $2.7 \times 10^{-9}$ moles/cm$^2$ simulating a polycrystalline platinum surface. The thick (2 $\mu$m) platinum coating on top of a nonporous $Al_2O_3$ support should closely resemble such a surface.

Although the original model included thermal radiation from the hot catalyst plates and one-dimensional heat conduction inside the solid catalyst plates, no such addition was necessary here; the thermocouple-measured catalyst temperature distribution serves as a wall boundary condition. The independent control of the two resistance heaters made it possible to attain temperature profiles in both plates differing by a maximum of only 8 K; the two measured streamwise temperature profiles were then averaged, and the resulting profile was used as a wall boundary condition for computations performed over half the channel width. Gravity was not included because it was found to have no influence for the Reynolds numbers of this study. The inlet boundary conditions were uniform profiles for the temperature (measured), the streamwise velocity (deduced from the measured temperature and mass flow rate), and the species mass fractions. Finally, zero Neumann outflow boundary conditions are used for the gas-phase variables and the no-slip condition at the wall for both velocity components.

The governing equations for the gas-phase variables were solved using a finite-volume approach. An orthogonal staggered grid of 99 $\times$ 25 points ($x$ and $y$, respectively) was used with variable spacing in both directions. The system of algebraic discretized equations for the gas-phase unknowns was solved iteratively using an ADI [14] algorithm. Surface coverages are coupled to the gas-phase variables via the interfacial boundary conditions. After a step for all gas-phase variables was completed, the surface coverage equations and the interfacial species boundary conditions were solved for every wall element using a modified Newton's method. The computational time was 12 h on a Sun-Ultra 1 workstation. When computations were performed with noncatalytic wall surfaces, an adaptive grid was necessary to capture the resulting strong flame.

## Results and Discussion

Results are presented for three catalytic cases further denoted as (a), (b), and (c) with incoming equivalence ratios ($\varphi$), velocities ($U_{IN}$), and temperatures ($T_{IN}$) as follows: for case (a), $\varphi = 0.37$, $U_{IN} = 1$ m/s, $T_{IN} = 750$ K; for case (b), $\varphi = 0.37$, $U_{IN} = 2$ m/s, $T_{IN} = 729$ K; and for case (c), $\varphi = 0.31$, $U_{IN} = 1$ m/s, $T_{IN} = 754$ K. The Reynolds number (based on the incoming properties and the channel hydraulic diameter) was about 186 for cases (a) and (c) and 390 for case (b). The incoming temperatures are slightly different as they are ultimately linked to the heat-transfer processes inside the channel. Figure 2 presents, for all cases, streamwise profiles of measured catalyst wall temperatures and computed mean (averaged over the channel cross section) gas temperatures, methane, and OH mass fractions. Homogeneous ignition is manifested by the sharp rise of the mean temperature or mean OH profiles. Homogeneous ignition takes place at $x = 72$ mm, 141 mm, and 76 mm for (a), (b), and (c), respectively, showing a weak dependence on equivalence ratio and a much stronger one on incoming velocity. Following homogeneous ignition, the mean methane mass fraction falls sharply, and practically all of the fuel is consumed within a few millimeters; at the channel exit, 100% conversion is achieved in all cases, with the heterogeneous contribution amounting to 73.7%, 70.7%, and 74.1% for (a), (b), and (c), respectively. Due to the high wall temperatures already from the leading edge of the plate ($T_{wall} >$ 1250 K at $x = 0$ in all cases), the surface reactions become quickly mass transport limited. This is also seen in Fig. 3, which presents, for case (a) only, transverse profiles of temperature and methane mass fraction at six selected streamwise distances; at

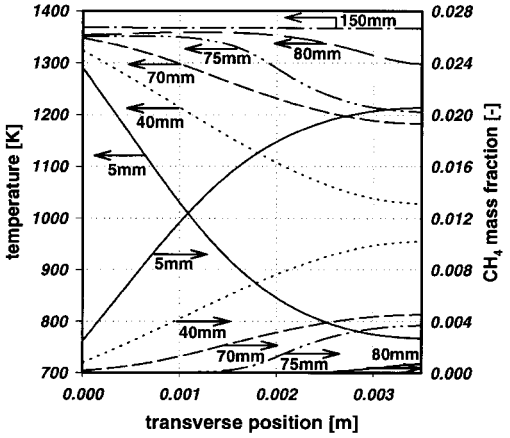


FIG. 3. Transverse profiles of temperature and methane mass fractions at six selected streamwise locations, case (a).

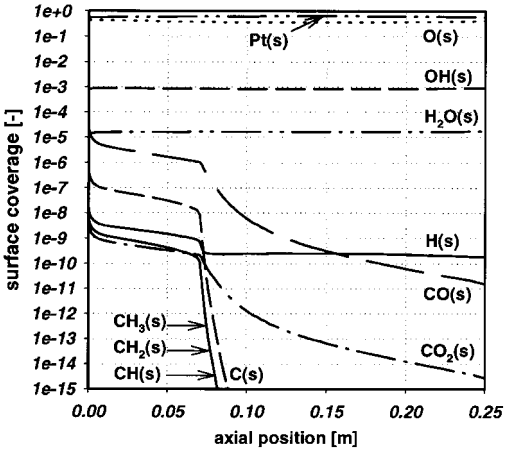


FIG. 5. Streamwise profile of surface coverage for case (a). Surface-bound species are indicated by (s).

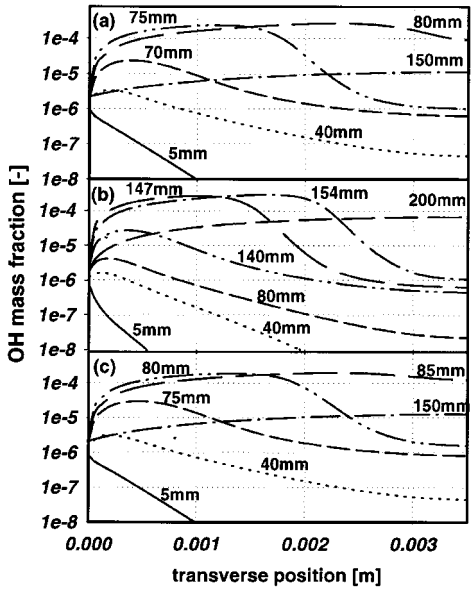


FIG. 4. Transverse profiles of OH mass fractions at six streamwise locations for cases (a), (b), and (c).

$x = 5$ mm, the wall ($y = 0$) methane concentration has already dropped to about 12% of its centerline value. For case (c), the same percentage is found, whereas for case (b), with increased mass transport coefficients due to its higher Reynolds number, the corresponding wall concentration is 16% of its centerline value. Following homogeneous ignition, the slope of the wall temperature gradient becomes positive (see Fig. 3), indicating heat transfer from the gas to the plate. The wall gradient slopes are also positive after ignition in case (b), whereas for the leaner case (c), the wall temperature slopes remain negative throughout the channel. The foregoing shows the inapplicability of van't Hoff's criterion (zero transverse wall temperature gradient) as a general means for defining the onset of homogeneous ignition in catalytic combustion.

Transverse profiles of the OH radical are given for all cases in Fig. 4. The slope of the OH radical changes from negative (net desorptive) to positive (net adsorptive) well before homogeneous ignition in all cases, indicating that gas-phase chemistry precedes any significant homogeneous heat release. Hence, homogeneous ignition criteria based on the shift of the OH peak in the transverse profiles from the wall to the gas phase are also inapplicable. The previous discussion shows that the streamwise changes in average quantities such as the sharp rise of mean temperature or of mean OH seen in Fig. 2 are better suited for a definition of homogeneous ignition than changes of local transverse wall gradients.

The streamwise surface coverage for case (a) is presented in Fig. 5. The surface is covered primarily with Pt(s) and O(s) over its entire length. The wall temperature is crucial in determining the Pt(s)/O(s) ratio. Due to the high sticking coefficient of oxygen, adsorption of oxygen is favored at lower temperatures resulting in a surface covered almost exclusively with O(s), which inhibits heterogeneous ignition. A rise in wall temperature shifts the adsorption and desorption equilibrium of oxygen to desorption, thus releasing free platinum sites on which methane can dissosiatively adsorb. For the high wall temperatures of this study, no oxygen inhibition was present; enough free platinum sites were available already from the leading edge (the surface coverage of platinum is $\Theta_{Pt} = 0.55$ at $x = 0$). The O(s) profile is largely controlled by the surface temperature; it

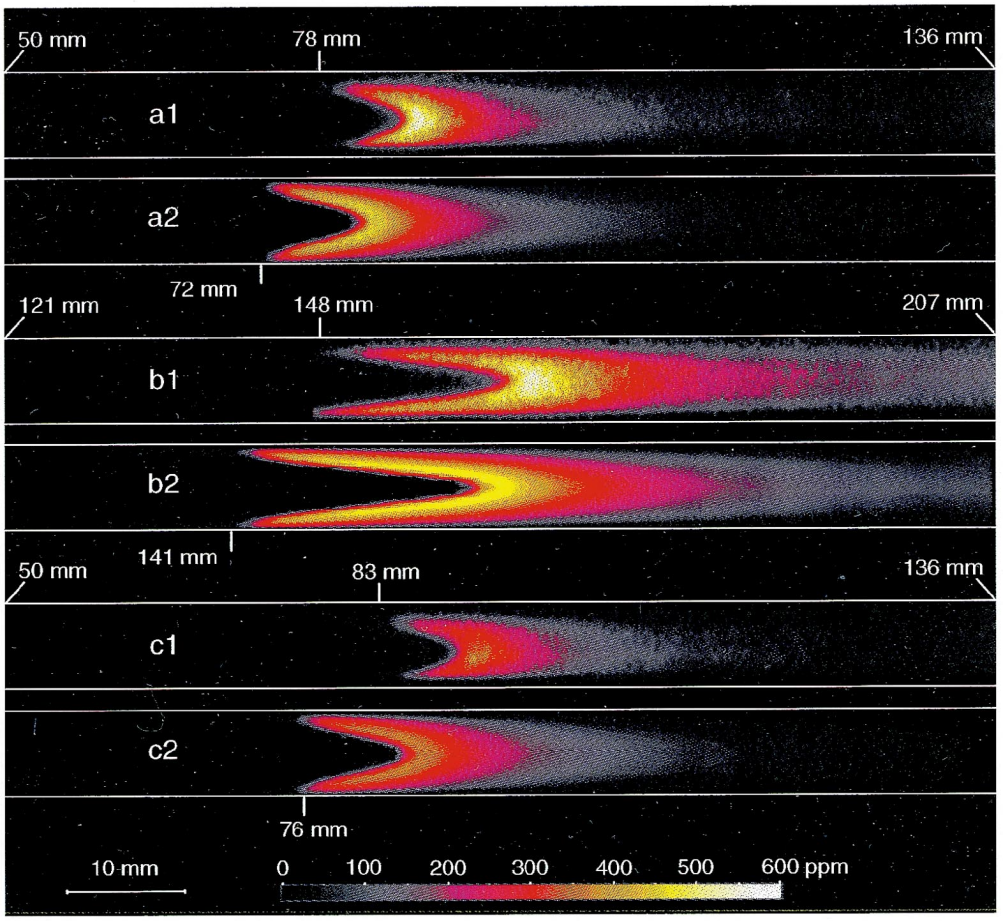


FIG. 6. Measured (a1, b1, c1) and predicted (a2, b2, c2) OH concentration maps (in ppm) for cases (a), (b), and (c), respectively. The tic marks at the beginning and end of each figure indicate the section of the channel shown. Vertical tic marks also indicate the measured and predicted homogeneous ignition locations.

has its lowest value near the center of the channel ($\Theta_O = 0.36$ at $x = 150$ mm), where the wall temperature is highest, and its highest values at the plate edges, where the wall temperature is lowest ($\Theta_O = 0.45$ at $x = 0$ and $\Theta_O = 0.41$ at $x = 250$ mm). All carbon-containing surface coverages drop sharply after homogeneous ignition. The foregoing discussion on surface coverage applies qualitatively to the other two cases.

In Fig. 6, PLIF-measured and predicted two-dimensional OH concentration maps are presented for all cases. Each measured PLIF image of Fig. 6 is an average over 100 laser shots. The reproducibility of the flame position and shape over extended times was excellent. The color-coded bar at the bottom of Fig. 6 provides the absolute levels of OH (in ppm) measured and computed. The OH calibration with the transverse laser sheet served also as a means to assess the two-dimensionality of the flame. Transverse OH visualization indicates that there is an extended (about 6 cm in width) central zone where two-dimensionality prevails, and only the zones extending 2 cm from each quartz window show a distinct three-dimensional saddle shape due to the increased heat losses. The predicted and measured homogeneous ignition locations in Fig. 6 are in good agreement with each other. Homogeneous ignition is underpredicted by 6 mm in (a) and by 7 mm in (b) and (c). It must be emphasized that accurate prediction of homogeneous ignition is very important in $NO_x$ emission calculations [15]. The sweep angle of the V-shaped flames is very well predicted, although the near-wall tails of the measured V-shaped flames are not well reproduced due to thermal radiation interference. For the low OH levels of all conditions and the high-pass filter used for signal collection,

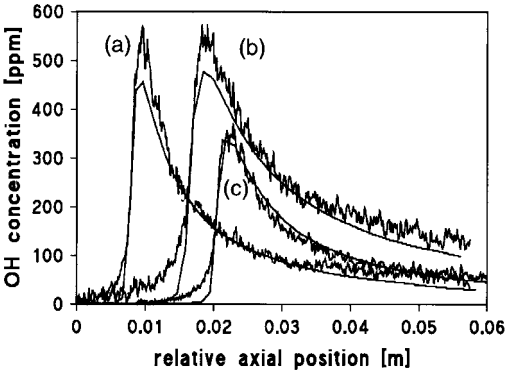


FIG. 7. Streamwise centerline OH profiles measured and predicted after homogeneous ignition for cases (a), (b), and (c). The predicted profiles have been sifted axially to match the measured peak OH locations. The predictions correspond to the smooth lines.

subtraction of the intense thermal radiation of the plates introduced significant errors; thermal radiation affected a zone extending about 0.9 mm from each plate. It must be stated, however, that the thermal radiation interference did not influence the OH calibration procedure, as the transverse laser sheet was kept at a safe distance from both walls. Absolute measured OH levels are in quite good agreement with the predictions given the uncertainties in the OH absorption calibration. Figure 7 presents measured and predicted centerline OH profiles, the latter shifted axially to match the measured peak OH locations; the relaxation of the OH toward its equilibrium value downstream of the flame is very well predicted. The overall model performance is hence considered very good, and in addition, the surface chemistry mechanism appears to capture the coupling between surface and gaseous chemistries leading to homogeneous ignition.

Computations were also performed with different values of the surface site density because this was the only experimental input not directly measured. The site density was decreased by a factor of 2 resulting only in small differences (2-mm earlier homogeneous ignition). A twofold increase in site density has almost no effect to the calculated homogeneous ignition location as surface reactions are close to their mass transport limit.

Finally, experiments and predictions were also carried out with inert Si[SiC] plates in a new case (d) with the following inlet conditions: $\varphi = 0.33$, $U_{IN} = 2.1$ m/s, and $T_{IN} = 680$ K. Predicted and PLIF-measured OH distributions are given in Fig. 8. Although the measured and predicted spread angles are very close to each other, the measured flame does not form a V-shape but a nearly planar one extending between both plates. The measured flame anchoring point is always at $x = 151$ mm (underpredicted by 7 mm), but its location in either the top or bottom plate is random; the shape of Fig. 8 (d1) randomly reverts to its symmetric counterpart with anchoring at the lower plate. The inert case is thus very sensitive to the boundary conditions. On the other hand, catalytically assisted combustion provides strong wall boundary conditions resulting in increased flame stability. The OH levels are much higher in the inert case (peak computed levels 3700 ppm and peak measured 4000 ppm). This is a result of the higher near-wall $CH_4$ concentration in the inert case owing to the absence of fuel depletion by surface reactions. In addition, the OH levels in the inert case peak near the wall resulting in a much stronger PLIF signal with no thermal radiation interference. The position of the homogeneous ignition ($x = 151$ mm) does not imply that the inert case

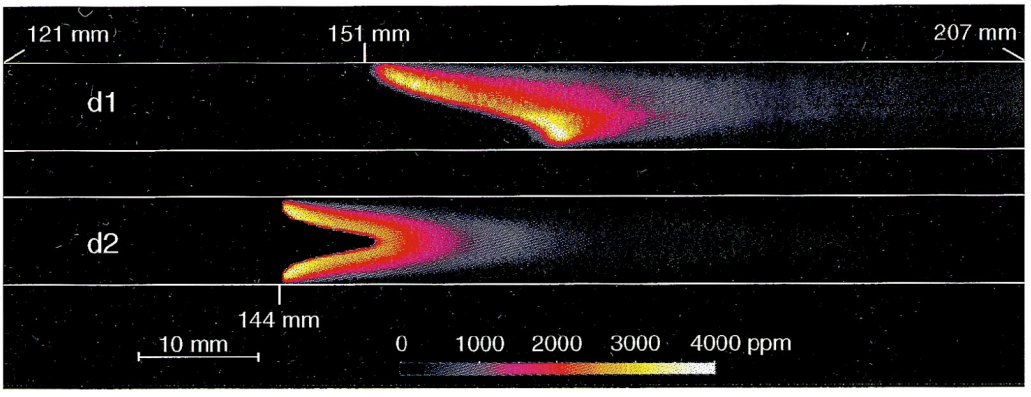


FIG. 8. Measured (d1) and predicted (d2) OH concentration maps (in ppm) for the noncatalytic case (d). The tic marks at the beginning and end of each figure indicate the section of the channel shown. Vertical tic marks also indicate the measured and predicted homogeneous ignition locations.

(d) ignites later than its catalytic counterpart as one might infer by comparing case (d) with the catalytic case (b). Although cases (d) and (b) have nearly the same inlet velocity and the effect of different equivalence ratios was shown to have no significant influence on the homogeneous ignition location, the wall temperature profiles in case (d) are about 150 K lower than the corresponding ones of case (b). An attempt to match the wall temperature profiles of any catalytic case moves the homogeneous ignition directly at the channel entrance because the near wall mixture has much higher $CH_4$ levels compared to the catalytic cases where fuel is depleted via surface reactions.

## Concluding Remarks

The catalytically stabilized thermal combustion (CST) of lean methane-air mixtures was investigated experimentally and numerically in a laminar plane channel flow with Pt-coated surfaces. The simulations included a two-dimensional elliptic model with detailed heterogeneous and homogeneous chemistries and the measurements PLIF of the OH radical and thermocouple monitoring of the catalyst surface temperature. Results indicate that the homogeneous ignition location is strongly influenced by the incoming velocity and mildly by the equivalence ratio. Very stable V-shaped flames are formed following homogeneous ignition. Measured flame sweep angles and absolute OH levels are in good agreement with predictions. In addition, the homogeneous ignition distance is predicted within 9% in all examined cases. The homogeneous ignition location is shown to be better identified with changes in averaged (over the channel cross section) quantities rather than with changes in local wall gradients. The overall model performance is quite good, suggesting that the surface scheme is adequate in capturing the coupling between gaseous and surface chemistries responsible for homogeneous ignition. Finally, experiments and predictions were carried with inert plate surfaces. The resulting strong flame is nearly planar and unstable, thus clearly showing the stability advantages of CST combustion.

### *Acknowledgments*

Support for this work was provided by the Swiss Federal Department of Energy (BEW). We also acknowledge the useful discussions with Professor H. B. Bockhorn of Karlsruhe University.

## REFERENCES

1. Ikeda, H., Libby, P. A., Williams, F. A., and Sato, J., *Combust. Flame* 93:138–148 (1993).
2. Bui, P. A., Vlachos, D. G., and Westmoreland, P. R., in *Twenty-Sixth Symposium (International) on Combustion,* The Combustion Institute, Pittsburgh, 1996, pp. 1763–1770.
3. Griffin, T. A., Pfefferle, L. D., Dyer, M. J., and Crosley, D. R., *Combust. Sci. Technol.* 65:19–37 (1989).
4. Markatou, P., Pfefferle, L. D., and Smooke, M. D., *Combust. Sci. Technol.* 79:247–268 (1991).
5. Bruno, C., Walsh, P. M., Santavicca, D. A., Sinha, N., Yaw, Y., and Bracco, F. V., *Combust. Sci. Technol.* 31:43–74 (1983).
6. Buser, S., Benz, P., Schlegel, A., and Bockhorn, H., *Ber. Bunsen-Ges. Phys. Chem.* 97(12):1719–1723 (1993).
7. Hellsing, B., Kasemo, B., and Zhdanov, V. P., *J. Catalysis* 132:210–228 (1991).
8. Behrendt, F., Deutschmann, O., Maas, U., and Warnatz, J., *J. Vacuum Sci. Technol. A* 13(3):1373–1377 (1995).
9. Dogwiler, U., Benz, P., and Mantzaras, J., "Two-Dimensional Modeling for Catalytically Stabilized Combustion of a Lean Methane-Air Mixture with Elementary Homogeneous and Heterogeneous Chemical Reactions," *Combust. Flame* 116:243–258 (1999).
10. Kee, R. J., Dixon-Lewis, G., Warnatz, J., Coltrin, M. E., and Miller, J. A., *A Fortran Computer Code Package for the Evaluation of Gas-Phase Multicomponent Transport Properties,* Sandia report SAND86-8246, July 1996 reprint.
11. Warnatz, J. and Maas, U., *Technische Verbrennung,* Springer-Verlag, New York, 1993, pp. 101–102.
12. Deutschmann, O., Behrendt, F., and Warnatz, J., *Catalysis Today* 21:461–470 (1994).
13. Warnatz, J., Allendorf, M. D., Kee, R. J., and Coltrin, M. E., *Combust. Flame* 96:393–406 (1994).
14. Srivatsa, S. K., "Cham Computer Code 201, CORA2—A Computer Code for Axisymmetrical Combustion Chambers," CHAM TR 201/1, 1977.
15. Schlegel, A., Benz, P., Griffin, T., Weisenstein, W., and Bockhorn, H., *Combust. Flame* 105:332–340 (1996).

# COMMENTS

*Dave Zerkle, Los Alamos National Laboratory, USA.* In a system with inert walls, the mechanism for homogeneous flame stabilization seems to be propagation in the low-velocity regions near the wall, that is, the boundary layer. Have you made any effort to validate the boundary-layer growth predicted by your CFD code? It seems that a difference in the predicted and experimental boundary-layer profiles might help to explain differences in the homogeneous ignition location.

*Author's Reply.* We do not attribute the small (4.6%) difference between predicted and measured inert-wall ignition distances to CFD considerations. There are experimental factors that can readily account for the observed difference. The most important factor is the accuracy in the thermocouple-measured wall temperature profile. Ignition distances are sensitive to the wall temperature because of their exponential dependence on it [1]. The thermocouples are embedded 1 mm beneath the channel wall that, as stated in the burner geometry section, can result to a few degrees difference between the actual and the measured channel wall temperature profiles. The CFD code has been extensively validated for both the momentum and the thermal boundary-layer development and the resulting local skin friction and heat-transfer coefficients in 2-D plane channel flow configurations. Moreover, the good agreement between the measured and the calculated flame sweep angle shown in Fig. 8 further points to a correct prediction of the boundary-layer growth in the channel.

## REFERENCE

1. Law, C. K. and Law, H. K., *Combust. Sci. Technol.* 25:1–8 (1981).

•

*Robert J. Kee, Colorado School of Mines, USA.* Often, it is desirable in catalytic combustion to suppress the homogeneous reaction so that essentially all combustion takes place on the surface. Do you see a way to extend your measurement technique to situations in which the OH concentration is very low? Such measurements would be quite valuable in understanding purely heterogeneous combustion.

*Author's Reply.* We agree that the measurement of radical concentrations inside the boundary layer is very important in the case of purely heterogeneous combustion. We add that such information is also of great importance for the combined heterogeneous–homogeneous combustion of this study, as it can shed light to the preignition processes that are important for the onset of homogeneous ignition. For this purpose, we are currently evaluating techniques capable of detecting sub-ppm levels of radical concentrations.

•

*Andrzej Teodorczyk, Warsaw University of Technology, Poland.* It seems that surface chemistry is the key problem in this process. Do you think that your mathematical model that involves several approximations is capable of verifying the adequacy of the surface chemistry kinetics used in your work?

*Author's Reply.* The surface chemistry scheme cannot be solely validated with the flame studies of this work. The homogeneous ignition distance presents a global parameter, and even if a perfect agreement between measured and predicted ignition distances could be achieved, it could not by itself serve as a validation tool for the surface chemistry. Given the sensitivity of the homogeneous ignition distance to many surface reactions (discussed in Ref. 9 of the paper), the good agreement between measured and predicted ignition distances strengthens the "validity" of the surface chemistry scheme, but it does not conclusively prove it. Heterogeneous ignition predictions using the same surface chemistry scheme were shown to be in good agreement with measurements [1]. We believe that a combination of studies like ours and [1] supplemented with fundamental research on the surface processes will eventually lead to well-understood surface reaction schemes. Finally, we do not agree with the statement that the mathematical model involves several approximations. The model as described in the paper is very detailed in the description of both the flow (elliptic approach) and the chemistry (full gaseous and surface chemistries).

## REFERENCE

1. Deutschmann, O., Schmidt, R., Behrendt, F., and Warnatz, J., in *Twenty-Sixth Symposium (International) on Combustion,* The Combustion Institute, Pittsburgh, 1996, pp. 1747–1754.